

Climate Variability: Nonlinear and Random Effects

Michael Ghil

Ecole Normale Supérieure, Paris, France, and
University of California, Los Angeles, USA

February 2012

Abstract. Nonlinear and random effects are pervasive in the atmospheric, oceanic and climate sciences. This article gives a unified treatment of such effects from the point of view of the theory of dynamical systems and of their bifurcations. Energy balance models are used to illustrate multiple equilibria, while multi-decadal oscillations in the thermohaline circulation illustrate the transition from steady states to periodic behavior. Random effects are introduced in the setting of random dynamical systems, which permit a unified treatment of both nonlinearity and stochasticity. This treatment is applied to a stochastically perturbed version of the classical Lorenz convection model.

Encyclopedia of the Atmospheric Sciences, 2nd edition,
G.R. North, F. Zhang and J. Pyle (Eds.)
Elsevier, accepted

Introduction

The global climate system is composed of a number of subsystems — atmosphere, biosphere, cryosphere, hydrosphere and lithosphere — each of which has distinct characteristic times, from days and weeks to centuries and millennia. Each subsystem, moreover, has its own internal variability, all other things being constant, over a fairly broad range of time scales. These ranges overlap between one subsystem and another. The interactions between the subsystems thus give rise to climate variability on all time scales.

We outline here the rudiments of the way in which *dynamical systems theory* is starting to provide an understanding of this vast range of variability. Such an understanding proceeds through the study of successively more complex patterns of behavior. These spatio-temporal patterns are studied within narrower ranges of time scales, such as *intraseasonal*, *interannual*, *interdecadal* and *multi-millennial*; each of these frequency bands is covered in a separate article of this Encyclopedia. The main results of dynamical systems theory that have demonstrated their importance for the study of climate variability involve *bifurcation theory* and the *ergodic theory* of dynamical systems. Since the first edition of this encyclopedia, the theory of *random dynamical systems* has made substantial contributions as well, and we account here for these as well.

In the next section, we describe the climate system's dominant balance between incoming solar radiation, dominated by short waves, and outgoing terrestrial radiation, dominated by long waves. This balance is consistent with the existence of *multiple equilibria* of surface temperatures. Such multiple equilibria are also present for other balances of climatic actions and reactions. Thus, on the intraseasonal time scale, the thermal driving of the mid-latitude westerly winds is countered by surface friction and mountain drag. Multiple equilibria typically arise from *saddle-node bifurcations* of the governing equations.

Transitions from one equilibrium to another may result from small and random pushes — a typical case of minute causes having large effects in the long term.

In the following section, we sketch the ocean's overturning circulation between cold regions, where water is heavier and sinks, and warm regions, where it is lighter and rises. The effect of temperature on the water masses' density and, hence, motion is in competition with the effect of salinity: density increases, through evaporation and brine formation, compete further with decreases in salinity and, hence, density through precipitation and river run-off. These competing effects can also give rise to two distinct equilibria.

In the present-day oceans, a *thermohaline* circulation prevails, in which the temperature effects dominate. In the remote past, about 50 Myr ago, a *halothermal* circulation may have obtained, with salinity effects dominating. In a simplified mathematical setting, these two equilibria arise by a *pitchfork bifurcation* that breaks the problem's mirror symmetry. On shorter time scales, of decades-to-millennia, *oscillations* of intensity and spatial pattern in the thermohaline circulation seem to be the dominant mode of variability. We show how interdecadal oscillations in the ocean's circulation arise by *Hopf bifurcation*.

In the final section, we address the way that faster processes, modeled as random effects, can interact with the slower, nonlinear ones. The combined treatment of the nonlinear and stochastic processes can reveal amazingly fine structure in the climate system's behavior, but also — and rather surprisingly — add robustness and predictability to the results. Concluding remarks follow.

Energy-Balance Models and the Modeling Hierarchy

The methods of dynamical systems theory have been applied first to simple models of atmospheric and oceanic flows, starting about forty years ago. More powerful computers now allow their application to fairly realistic and detailed models of the atmosphere, ocean, and the coupled atmosphere–ocean system. We start therefore by presenting such a hierarchy of models.

This presentation is interwoven with that of the *successive bifurcations* that lead from simple to more complex solution behavior for each climate model. Useful tools for comparing model behavior across the hierarchy and with observations are provided by ergodic theory. Among these, advanced methods for the analysis and prediction of uni- and multivariate time series play an important role.

Radiation balance and energy-balance models (EBMs)

At present, the best-developed hierarchy is for atmospheric models. Atmospheric models were originally developed for weather simulation and prediction on the time scale of hours to days. Currently they serve — in a stand-alone mode or coupled to oceanic and other models — to address climate variability on all time scales.

The first rung of the modeling hierarchy for the atmosphere is formed by zero-dimensional (0-D) models, where the number of dimensions, from zero to three, refers to the number of independent space variables used to describe the model domain, *i.e.* to physical-space dimensions. Such 0-D models essentially attempt to follow the evolution of global surface-air temperature \bar{T} as a result of changes in global radiative balance:

$$c \frac{d\bar{T}}{dt} = R_i - R_o, \quad [1a]$$

$$R_i = \mu Q_0 \{1 - \alpha(\bar{T})\}, \quad R_o = \sigma m(\bar{T})\bar{T}^4. \quad [1b, c]$$

Here R_i and R_o are incoming solar radiation and outgoing terrestrial radiation. The heat capacity c is that of the global atmosphere, plus that of the global ocean or some fraction thereof, depending on the time scale of interest: one might only include in c the ocean mixed layer when interested in subannual time scales but the entire ocean when studying paleoclimate. The rate of change of \bar{T} with time t is given by $d\bar{T}/dt$, while Q_0 is the solar radiation received at the top of the atmosphere, s is the Stefan–Boltzmann constant, and m is an insolation parameter, equal to unity for present-day conditions. To have a closed, self-consistent model, the planetary reflectivity or albedo α and grayness factor m have to be expressed as functions of \bar{T} ; $m = 1$ for a perfectly black body and $0 < m < 1$ for a grey body like planet Earth.

There are two kinds of one-dimensional (1-D) atmospheric models, for which the single spatial variable is latitude or height, respectively. The former are so-called *energy-balance models* (EBMs), which consider the generalization of the model (2.1) for the evolution of surface-air temperature $T = T(x,t)$, say,

$$c(x) \frac{\partial T}{\partial t} = R_i - R_o + D. \quad [2]$$

Here the terms on the right-hand side can be functions of the meridional coordinate x (latitude, co-latitude, or sine of latitude), as well as of time t and temperature T . The horizontal heat-flux term D expresses heat exchange between latitude belts; it typically contains first and second partial derivatives of T with respect to x . Hence the rate of change of local temperature T with respect to time also becomes a partial derivative, $\partial T / \partial t$.

The first striking results of theoretical climate dynamics were obtained in showing that Eq. [2] could have two stable steady-state solutions, depending on the value of the insolation

parameter μ , cf. Eq. [1b]. This multiplicity of stable steady states, or physically possible “climates” of our planet, can be explained, in its simplest form, in the 0-D model [1]. The simple explanation resides in the fact that — for a fairly broad range of μ -values around $\mu = 1.0$ — the curves for R_i and R_o as a function of \bar{T} intersect in 3 points. One of these corresponds to the present climate (highest \bar{T} -value), and another one to an ice-covered planet (lowest \bar{T} -value); both of these are stable, while the third one (intermediate \bar{T} -value) is unstable. To obtain this result, it suffices to make two assumptions: (i) that $\alpha = \alpha(\bar{T})$ is a piecewise-linear function of \bar{T} , with high albedo at low temperature, due to the presence of snow and ice, and low albedo at high \bar{T} , due to their absence; and (ii) that $m = m(\bar{T})$ is a smooth, increasing function of \bar{T} that attempts to capture in its simplest form the “greenhouse effect” of trace gases and water vapor.

The *bifurcation diagram* of such a 1-D EBM is shown in Fig. 1. It displays the model’s mean temperature \bar{T} as a function of the fractional change μ in the insolation $Q = Q(x)$ at the top of the atmosphere. The ‘S’-shaped curve in the figure arises from two back-to-back saddle-node bifurcations. The *normal form* of the first one is

$$\dot{X} = \mu - X^2. \quad [3]$$

Here X stands for a suitably normalized form of \bar{T} and $\dot{X} \equiv dX/dt$ is the rate of change of X , while μ is a parameter that measures the stress on the system, in particular a normalized form of the insolation parameter.

[Fig. 1 near here, please.]

The uppermost branch corresponds to the steady-state solution $X = +\mu^{1/2}$ of Eq. [3] and is stable. It matches rather well Earth’s present-day climate for $\mu = 1.0$, more precisely the steady-state solution $T = T(x; \mu)$ of the full 1-D EBM (not shown) matches closely the annual

mean temperature profile from instrumental data over the last century.

The intermediate branch starts out at the left as the second solution, $X = -\mu^{1/2}$, of Eq. [3] and is unstable. It blends smoothly into the upper branch of a coordinate-shifted and mirror-reflected version of Eq. [3], say

$$\dot{X} = \mu - \mu_0 + (X - X_0)^2. \quad [4]$$

This branch, $X = X_0 + (\mu_0 - \mu)^{1/2}$, is also unstable. Finally, the lowermost branch in Fig. 1 is the second steady-state solution of Eq. [4], $X = X_0 - (\mu_0 - \mu)^{1/2}$, and is also stable. It corresponds to an ice-covered planet at the same distance from the Sun as Earth.

The fact that the upper-left bifurcation point (μ_c, T_c) in Fig. 1 is so close to present-day insolation values created great concern in the climate dynamics community in the mid-1970s, when these results were obtained. Indeed, much more detailed computations (see below) confirmed that a reduction of about 2–5% of insolation values would suffice to precipitate Earth into a “deep freeze.” The great distance of the lower-right bifurcation point (μ_d, T_d) from present-day insolation values, on the other hand, suggests that one would have to nearly double atmospheric opacity, say, for the Earth’s climate to jump back to more comfortable temperatures.

Other atmospheric processes and models

The 1-D atmospheric models in which the details of radiative equilibrium are investigated with respect to a height coordinate z (geometric height, pressure, etc.) are often called *radiative-convective models*. This name emphasizes the key role that convection plays in vertical heat transfer. While these models preceded historically EBMs as rungs on the modeling hierarchy, it was only recently shown that they, too, could exhibit multiple

equilibria. The word (stable) “equilibrium,” here and in the rest of this article, refers simply to a (stable) steady state of the model, rather than a true thermodynamic equilibrium.

Two-dimensional (2-D) atmospheric models are also of two kinds, according to the third space coordinate that is not explicitly included. Models that resolve explicitly two horizontal coordinates, on the sphere or on a plane tangent to it, tend to emphasize the study of the dynamics of large-scale atmospheric motions. They often have a single layer or two. Those that resolve explicitly a meridional coordinate and height are essentially combinations of EBMs and radiative-convective models and emphasize therewith the thermodynamic state of the system, rather than its dynamics.

Yet another class of “horizontal” 2-D models is the extension of EBMs to resolve zonal, as well as meridional surface features, in particular land-sea contrasts. We shall see in Section 3.2 how such a 2-D EBM is used, when coupled to an oceanic model.

Schneider and Dickinson (1974) and Ghil and Robertson (2000) discuss additional types of 1-D and 2-D atmospheric models and give references to these and to the types discussed above, along with some of their main applications (see Further Reading). Finally, to encompass and resolve the main atmospheric phenomena with respect to all three spatial coordinates, *general circulation models* (GCMs) occupy the pinnacle of the modeling hierarchy.

The dependence of mean zonal temperature on the insolation parameter μ (the normalized "solar constant") — as obtained for 1-D EBMs and shown in Fig. 1 here — was confirmed, to the extent possible, by using a simplified GCM, coupled to a “swamp” ocean model. More precisely, forward integrations with a GCM cannot confirm the presence of the intermediate, unstable branch. Nor was it possible in the mid-70s, when this numerical experiment was done, to reach the “deep-freeze” stable branch, because of the GCM’s

computational limitations. But the parabolic shape of the upper, present-day–like branch near the upper-left bifurcation point in our figure, cf. Eq. [3], was well supported by the GCM simulations.

Ghil and Robertson also describe the separate hierarchies that have grown over the last quarter-century in modeling the ocean and the coupled ocean–atmosphere system. More recently, an overarching hierarchy of earth-system models — that encompass all the subsystems of interest, atmosphere, biosphere, cryosphere, hydrosphere and lithosphere — has been developing. Eventually, the partial results about each subsystem’s variability, outlined in this section and the next one, will have to be verified from one rung to the next of the earth-system modeling hierarchy.

Interdecadal oscillations in the oceans’ thermohaline circulation

Theory and simple models

Historically, the thermohaline circulation (THC) was first among the climate system’s major processes to be studied using a very simple mathematical model. Stommel (1961) formulated a two-box model and showed that it possessed multiple equilibria.

A sketch of the Atlantic Ocean’s THC and its interactions with the atmosphere and cryosphere on long time scales is shown in Fig. 2. These interactions can lead to climate oscillations with multi-millennial periods, such as the Heinrich events, and are summarized in the figure’s caption. An equally schematic view of the global THC is provided by the widely known “conveyor belt” diagram. The latter diagram does not commonly include the THC’s interactions with water in both its gaseous and solid phases, which the former does include.

[Fig. 2 near here, please.]

Basically, the THC is due to denser water sinking, lighter water rising, and water-mass continuity closing the circuit through near-horizontal flow between the areas of rising and sinking. The effects of temperature and salinity on the ocean water's density, $\rho = \rho(T, S)$, oppose each other: the density ρ *decreases* with increasing T and *increases* with increasing S . It is these two effects that give the *thermohaline* circulation its name, from the Greek words for T and S . In high latitudes, ρ increases as the water loses heat to the air above and, if sea ice is formed, as the water underneath is enriched in brine. In low latitudes, ρ increases due to evaporation but decreases due to sensible heat flux into the ocean.

For the present climate, the temperature effect is stronger than the salinity effect, and ocean water is observed to sink in certain areas of the high-latitude North Atlantic and Southern Ocean — with very few and limited areas of deep-water formation elsewhere — and to rise everywhere else. Thus, in a *thermohaline* regime, T is more important than and hence comes before S . During some remote geological times, deep water may have formed in the global ocean near the equator; such an overturning circulation of opposite sign to that prevailing today has been dubbed *halothermal*, S before T . The quantification of the relative effects of T and S on the oceanic water masses' buoyancy in high and low latitudes is far from complete, especially for paleocirculations; the association of the latter with salinity effects that exceed the thermal ones is thus rather tentative.

Stommel considered a two-box model, with two pipes connecting the two boxes. He showed that the system of two nonlinear, coupled ordinary differential equations that govern the temperature and salinity differences between the two well-mixed boxes has two stable steady-state solutions, distinguished by the direction of flow in the upper and lower pipe. Stommel's paper was primarily concerned with distinct local convection regimes, and hence vertical stratifications, in the North Atlantic and Mediterranean (or Red Sea), say. Today, we

mainly think of one box as representing the low latitudes and the other one the high latitudes in the global THC.

The next step in the hierarchical modeling of the THC is that of 2-D meridional plane models, in which the temperature and salinity fields are governed by coupled nonlinear partial differential equations with two independent space variables, latitude and depth, say. Given boundary conditions for such a model that are symmetric about the Equator, as are the equations themselves, one expects a symmetric solution, in which water either sinks near the poles and rises everywhere else (thermohaline) or sinks near the Equator and rises everywhere else (halothermal). These two symmetric solutions would correspond to the two equilibria of Stommel's box model of 1961.

In fact, symmetry breaking can occur, leading gradually from a symmetric two-cell circulation to an antisymmetric one-cell circulation. In between, all degrees of dominance of one cell over the other are possible. A situation lying somewhere between the two seems to resemble most closely the meridional overturning diagram of the Atlantic Ocean in Fig. 2.

This symmetry breaking can be described by a *pitchfork bifurcation*:

$$\dot{X} = \mu X - X^3. \quad [5]$$

Here X stands for the amount of asymmetry in the solution, so that $X = 0$ is the symmetric branch, and μ is a parameter that measures the stress on the system, in particular a normalized form of the buoyancy flux at the surface. For $\mu < 0$ the symmetric branch is stable, while for $\mu > 0$ the two branches $X = \pm \mu^{1/2}$ inherit its stability.

In the 2-D THC problem, the left cell dominates on one branch, while the right cell dominates on the other: for a given value of μ , the two stable steady-state solutions — on the $\{X = + \mu^{1/2}\}$ branch and on the $\{X = - \mu^{1/2}\}$ branch — are mirror images of each other. The idealized THC in Fig. 2, with the North Atlantic Deep Water extending to the Southern

Ocean's polar front, corresponds to one of these two branches. In theory, therefore, a mirror-image circulation, with the Antarctic Bottom Water extending to the North Atlantic's polar front, is equally possible.

Bifurcation diagrams for GCMs

F. Bryan was the first, in 1986, to document transition from a two-cell to a one-cell circulation in a simplified ocean GCM with idealized, symmetric forcing. Results of coupled ocean–atmosphere GCMs, however, have led to questions about the realism of more than one stable THC equilibrium. The situation with respect to the THC's pitchfork bifurcation (3.1) is thus subtler than it was with respect to Fig. 1 for radiative equilibrium. In the previous section, atmospheric GCMs confirmed essentially the EBM results; the results obtained in climbing the rungs of the modeling hierarchy for the THC are still in need of further clarification.

Internal variability of the THC — with smaller and more regular excursions than the huge and totally irregular jumps associated with bistability — was studied intensively in the late 1980s and the 1990s. These studies placed themselves on various rungs of the modeling hierarchy, from box models through 2-D models and all the way to ocean GCMs. A summary of the different kinds of oscillatory variability found in the latter appears in Table I. Such oscillatory behavior seems to match more closely the instrumentally recorded THC variability, as well as the paleoclimatic records for the recent geological past, than bistability.

[Table I near here, please.]

The (multi)millennial oscillations interact with variability in the surface features and processes shown in Fig. 2. Chen and Ghil, in particular, studied some of the interactions between atmospheric processes and the THC. They used a so-called hybrid coupled model, namely a (horizontally) 2-D EBM, coupled to a rectangular-box version of the North Atlantic

rendered by a low-resolution ocean GCM. This hybrid model's regime diagram is shown in Fig. 3a. A steady state is stable for high values of the coupling parameter λ_{ao} or of the EBM's diffusion parameter d . Interdecadal oscillations with a period of 40–50 years are self-sustained and stable for low values of these parameters.

[Fig. 3 near here, please.]

The self-sustained THC oscillations in question are characterized by a pair of vortices of opposite sign that grow and decay in quadrature with each other in the ocean's upper layers. Their centers follow each other anti-clockwise through the northwestern quadrant of the model's rectangular domain. Both the period and the spatio-temporal characteristics of the oscillation are thus rather similar to those seen in a fully coupled GCM with realistic geometry. The transition from a stable equilibrium to a stable limit cycle, via Hopf bifurcation, in this hybrid coupled model, is shown in Fig. 3b.

Randomness and Nonlinearity

What to expect

The geometric and the ergodic theory of dynamical systems represent significant achievements of the 20th century. The foundations of the stochastic calculus in its second half also led to the birth of a rigorous theory of time-dependent random phenomena. Historically, theoretical developments in climate dynamics have been largely motivated by these two complementary approaches, based on the work of E. N. Lorenz and that of K. Hasselmann, respectively.

It now seems clear that these two approaches complement, rather than exclude each other. Incomplete knowledge of small-, subgrid-scale processes, as well as computational limitations will always require one to account for these processes in a stochastic way. As a

result of sensitive dependence on initial data and on parameters, numerical weather forecasts, as well as climate projections are both expressed these days in probabilistic terms. In addition to the intrinsic challenge of addressing the nonlinearity along with the stochasticity of climatic processes, it is thus more convenient — and becoming more and more necessary — to rely on a model's (or set of models') probability density function (PDF) rather than on its individual, point-wise simulations or predictions.

We summarize here results on the surprisingly complex statistical structure that characterizes stochastic nonlinear systems. This complex structure does provide meaningful physical information that is not described by the PDF alone; it lives on a *random attractor*, which extends the concept of a *strange attractor* and of its *invariant measures* from deterministic to stochastic dynamics.

What one finds

On the road to including random effects, one needs to realize first that the climate system — as well as any of its subsystems, and on any time scale — is not closed: it exchanges energy, mass and momentum with its surroundings, whether other subsystems or the interplanetary space and the solid earth. The typical applications of dynamical systems theory to climate variability so far have only taken into account exchanges that are constant in time, thus keeping the model — whether governed by ordinary, partial or other differential equations — *autonomous*; i.e., the models had coefficients and forcings that were constant in time.

Succinctly, one can write such a system as

$$\dot{\mathbf{X}} = \mathbf{f}(\mathbf{X}, \boldsymbol{\mu}), \quad [6]$$

where \mathbf{X} now may stand for any state vector or climate field, while \mathbf{f} is a smooth function of \mathbf{X} and of the vector of parameters $\boldsymbol{\mu}$, but does not depend explicitly on time. This characteristic

of being autonomous greatly facilitated the analysis of model solutions' properties. For instance, two distinct trajectories, $\mathbf{X}_1(t)$ and $\mathbf{X}_2(t)$, of a well-behaved, smooth autonomous system cannot pass through the same point in phase space, which helps describe the system's phase portrait. So does the fact that we only need to consider the behavior of solutions $\mathbf{X}(t)$ as we let time t tend to $+\infty$: the resulting sets of points are — possibly multiple — equilibria, periodic solutions, and chaotic sets. In the language of dynamical systems theory, these are called, respectively: *fixed points*, *limit cycles*, and *strange attractors*.

We know only too well, however, that the seasonal cycle plays a key role in climate variability on many time scales, while orbital forcing is crucial on the Quaternary time scales of many millennia, and now anthropogenic forcing is of utmost importance on interdecadal time scales. How can one take into account such time-dependent forcings, and analyze the nonautonomous systems, written succinctly as

$$\dot{\mathbf{X}} = \mathbf{f}(\mathbf{X}, t; \mu), \quad [7]$$

to which they give rise? In Eq. [7], the dependence of \mathbf{f} on t may be periodic, $\mathbf{f}(\mathbf{X}, t + P) = \mathbf{f}(\mathbf{X}, t)$ as in various El Niño–Southern Oscillation (ENSO) models, where the period $P = 12$ months, or monotone, $\mathbf{f}(\mathbf{X}, t + \tau) \geq \mathbf{f}(\mathbf{X}, t)$, as in studying scenarios of anthropogenic climate forcing.

To illustrate the fundamental character of the distinction between an autonomous system like [6] and a nonautonomous one like [7], consider the simple scalar version of these two equations:

$$\dot{X} = -\beta X, \quad [8]$$

and

$$\dot{X} = -\beta X + \sigma_0 t, \quad [9]$$

respectively. We assume that both systems are dissipative, i.e. $\beta > 0$, and that the forcing is

monotone increasing, $\gamma \geq 0$, as would be the case for anthropogenic forcing in the industrial era. Lorenz in his 1963 paper pointed out the key role of dissipativity in giving rise to strange, but attracting solution behavior, while M. Ghil and S. Childress in their 1987 book emphasized its importance and pervasive character in climate dynamics. Clearly the only attractor for the solutions of Eq. [6], given any initial point $X(0) = X_0$, is the fixed point $X = 0$, attained as $t \rightarrow +\infty$.

In the case of Eq. [9], though, this *forward-in-time approach* yields blow-up as $t \rightarrow +\infty$, for any initial point. To make sense of what happens in the case of time-dependent forcing, one introduces instead the *pullback approach*, in which solutions are allowed to still depend on the time t at which we observe them, but also on a time s from which the solution is started, $X(s) = X_0$; presumably $s \ll t$. With this little change of approach, one can easily verify that

$$|X(s, t; X_0) - A(t)| \rightarrow 0 \text{ as } s \rightarrow -\infty, \quad [10a]$$

for all t and X_0 , where

$$A(t) = \gamma(t - 1/\beta)/\beta. \quad [10b]$$

We thus obtain, in this pullback sense, the intuitively obvious result that the solutions, if we start them far enough in the past, all approach the attractor set $A(t)$, which has a linear growth in time, thus following the forcing.

Let us return now to the more general, nonlinear case of Eq. [7] and add not only deterministic time dependence $\mathbf{f}(\mathbf{X}, t)$, but also random forcing,

$$d\mathbf{X} = \mathbf{f}(\mathbf{X}, t)dt + \mathbf{g}(\mathbf{X})d\eta, \quad [11]$$

where $\eta = \eta(t, \omega)$ represents a Wiener process — commonly referred to as “white noise” — and ω labels the particular realization of this random process. The case $\mathbf{g}(\mathbf{X}) = \mathbf{const.}$ is the case of *additive noise*, while in the case of $\partial\mathbf{g}(\mathbf{X})/\partial\mathbf{X} \neq \mathbf{0}$ we speak of *multiplicative noise*. The

distinction between dt and $d\eta$ in Eq. [11] is necessary since, roughly speaking and following Einstein's celebrated 1905 paper on Brownian motion, it is the variance of a Wiener process that is proportional to time and thus $d\eta \propto (dt)^{1/2}$.

In the case of random forcing, the concepts introduced by the simple example of Eqs. [10a, b] above can be illustrated by the random attractor $\mathcal{A}(\omega)$ (yellow band) of Fig. 4. In the figure, $d\eta(t, \omega) = \theta(t)\omega$ is the random process that drives the system (solid black line) and the pullback attraction is depicted by the flow of an arbitrary set \mathbf{B} from "pullback times" $t = -\tau_2$ and $t = -\tau_1$ onto the attractor (heavy blue arrows).

More explicitly, we show in Fig. 5 four "snapshots" $\{A_j(\omega) = A(\omega; t = t_j) : j = 1, 2, 3, 4\}$ that correspond to the vertical cross-sections (heavy solid) in the attractor of Fig. 4; a short video, from which these snapshots are taken, is also linked to this article. These snapshots were calculated for the random attractor $\mathcal{A}(\omega)$ of a stochastically perturbed Lorenz system, given by

$$\begin{cases} dX = P_r(Y - X)dt + \sigma_0 X d\eta, \\ dY = (rX - Y - XZ)dt + \sigma_0 Y d\eta, \\ dZ = (-bZ + XY)dt + \sigma_0 Z d\eta. \end{cases} \quad [12]$$

The parameters r , P_r and b in Eq. [12] have the usual meanings for two dimensional thermal convection: $r = R/R_c$ is the Rayleigh number R normalized by its critical value R_c at the onset of convection, P_r is the Prandtl number, and b is a normalized wavenumber for the most unstable wave at the onset of convection. The noise in this case is multiplicative: its intensity $\sigma_0 = 0.5$ is multiplied in each one of the three coupled, nonlinear equations above by the corresponding variable X , Y or Z .

To be precise, what is plotted in Fig. 5, and in the associated video, is the density of the invariant measure $\nu(\omega)$ supported on the random attractor of the stochastically perturbed Lorenz system [12]. This measure indicates the probability of trajectories winding up in a

particular region of phase space and it is very highly concentrated on the attractor, as inferred from the huge range of density values: the color bar in the figure is on a logarithmic scale, and extends over more than 10 orders of magnitude. The situation is thus very different from that expected when studying additive noise — in that case, the noise tends to smear out the fine, Cantor–set-like structure of the deterministic, strange attractor and the associated PDF has nonzero-volume support.

It hardly needs saying that additive noise has been studied in climate dynamics much more extensively since it was easier to do so, and was suggested by the simple Brownian motion analogy of “weather = water molecules” and “climate = pollen particle,” as proposed by Hasselmann in 1976. Across the hierarchy of climate models discussed in the previous two sections of this article, however, it is clear that small-and-fast scales of motion do not enter exclusively in an additive manner: they pop up in many, if not all terms of the governing equations, as summarized in Eq. [11] above. The insights offered, therefore, by Fig. 5 and the video are likely to be of interest across the hierarchy of models, all the way up to coupled GCMs and Earth system models.

The invariant measure in Fig. 5 exhibits amazing complexity, with fine, very intense filamentation: there is no fuzziness whatsoever in the topological structure of this filamentation, which does evoke the Cantor-set foliation of the deterministic attractor. This fine structure strongly suggests that an object of vanishing volume supports this measure, i.e. that the random attractor $\mathcal{A}(\omega)$ of system [12] has — like the strange attractor of the classical, deterministic version, with $\sigma_0 = 0$ — dimension smaller than 3.

Such complexity, however, should not hide the fact that the theory of random dynamical systems provides robust tools for studying the parameter dependence of a nonlinear, randomly perturbed system’s various “metrics.” These metrics can include global quantities, like mean

temperature or total energy, but also much finer functionals of the state of the system, such as regional temperatures or precipitation. In addition, this theory can help improve prediction of future system properties, by relying on a judicious combination of the history of its slow and fast behavior.

Concluding Remarks

A complete theory of climate variability, across the entire range of time scales of interest, is still in the future. We have shown, though, that powerful conceptual and numerical tools exist in order to organize the emerging knowledge so far. The approach described herein relies on applying systematically dynamical systems theory, both deterministic and stochastic, across a hierarchy of models, from the simplest toy models to the most detailed, coupled GCMs. This approach has progressed from its first modest steps, taken almost exactly half-a-century ago, to the analysis of the behavior of atmospheric, oceanic and coupled GCMs over the last two decades. Particularly interesting strides have been taken over the last decade in studying the interaction of the faster time scales with the slower ones, within a genuinely nonlinear framework.

Further Reading

Arnold, L. (1998) *Random Dynamical Systems* (Springer-Verlag, New York/Berlin).

Bryan, F. (1986) High-latitude salinity effects and interhemispheric thermohaline circulations *Nature*, **323**, 301–304.

Chekroun, M. D., D. Kondrashov, and M. Ghil, 2011: Predicting stochastic systems by noise sampling, and application to the El Niño-Southern Oscillation, *Proc. Natl. Acad. Sci. USA*, [doi:10.1073/pnas.1015753108](https://doi.org/10.1073/pnas.1015753108).

Chekroun, M. D., E. Simonnet, and M. Ghil (2011) Stochastic climate dynamics: Random attractors and time-dependent invariant measures, *Physica D*, [doi:10.1016/j.physd.2011.06.005](https://doi.org/10.1016/j.physd.2011.06.005).

Chen, F., and M. Ghil (1996) Interdecadal variability in a hybrid coupled ocean-atmosphere model, *J. Phys. Oceanogr.*, **26**, 1561–1578.

Dijkstra, H. A. (2005) *Nonlinear Physical Oceanography: A Dynamical Systems Approach to the Large-Scale Ocean Circulation and El Niño*, 2nd ed. (Kluwer Acad. Publishers, Dordrecht/Norwell, Mass.) 532 pp.

Eckmann, J.-P., and D. Ruelle (1985) Ergodic theory of chaos and strange attractors. *Rev. Mod. Phys.*, **57**, 617-656 (addendum, *Rev. Mod. Phys.*, **57**, 1115).

Einstein, A., 1905: On the movement of small particles suspended in a stationary liquid demanded by the molecular-kinetic theory of heat. *Ann. d. Physik* (Leipzig), **17**, 549 ff., reprinted in *Investigations on the Theory of the Brownian Movement*, five articles by A. Einstein, R. Fürth (Ed.) and A. D. Cowper (transl.), 1956, Dover Publ., New York, 122 pp.

Ghil, M. (1994) Cryothermodynamics: The chaotic dynamics of paleoclimate, *Physica D*, **77**, 130–159.

Ghil, M., and S. Childress (1987) *Topics in Geophysical Fluid Dynamics: Atmospheric Dynamics, Dynamo Theory and Climate Dynamics* (Springer-Verlag, New York/Berlin).

Ghil, M., and A. W. Robertson (2000) Solving problems with GCMs: General circulation models and their role in the climate modeling hierarchy, in *General Circulation Model Development: Past, Present and Future*, D. Randall (Ed.), Academic Press, San Diego, pp. 285–325.

Ghil, M., A. Mullhaupt and P. Pestiaux (1987) Deep water formation and Quaternary glaciations, *Climate Dyn.*, **2**, 1–10.

Ghil, M., M. R. Allen, M. D. Dettinger, K. Ide, D. Kondrashov, M. E. Mann, A. W. Robertson, A. Saunders, Y. Tian, F. Varadi, and P. Yiou (2002) Advanced spectral methods for climatic time series, *Rev. Geophys.*, **40**(1), pp. 3.1–3.41, [doi: 10.1029/2000RG000092](https://doi.org/10.1029/2000RG000092).

Ghil, M., M. D. Chekroun, and E. Simonnet, 2008: Climate dynamics and fluid mechanics: Natural variability and related uncertainties, invited survey paper for Special Issue on “*The Euler Equations: 250 Years On*,” *Physica D*, **237**, 2111–2126, [doi:10.1016/j.physd.2008.03.036](https://doi.org/10.1016/j.physd.2008.03.036).

Guckenheimer, J., and P. Holmes, *Nonlinear Oscillations, Dynamical Systems and Bifurcations of Vector Fields* (Springer-Verlag, New York/Berlin) 453 pp., 1983.

- Hasselmann, K. (1976) Stochastic climate models, Part I: Theory. *Tellus*, **28**, 473–485.
- Kalnay, E. (2003) *Atmospheric Modeling, Data Assimilation and Predictability*. Cambridge Univ. Press, Cambridge/London, UK, 341 pp.
- Lorenz, E. N. (1963) Deterministic nonperiodic flow. *J. Atmos. Sci.*, **20**, 130–141.
- Kennett, R. P., and L. D. Stott (1991) Abrupt deep-sea warming, paleoceanographic changes and benthic extinctions at the end of the Palaeocene, *Nature*, **353**, 225–229.
- Marotzke, J. (2000) Abrupt climate change and thermohaline circulation: Mechanisms and predictability, *Proc. Natl. Acad. Sci.*, **97**, 1347–1350.
- North, G. R., R. F. Cahalan and J. A. Coakley, Jr. (1981) Energy balance climate models, *Rev. Geophys. Space Phys.*, **19**, 91–121.
- Ramanathan, V., and J. A. Coakley (1978) Climate modeling through radiative convective models, *Rev. Geophys. Space Phys.*, **16**, 465–489.
- Ruelle, D., and F. Takens, 1971: On the nature of turbulence. *Commun. Math. Phys.*, **20**, 167–192, and **23**, 343–344.
- Schneider, S.H., and R.E. Dickinson (1974) Climate modeling, *Rev. Geophys. Space Phys.*, **25**, 447–493.
- Solomon, S., *et al.* (2007) *Climate Change 2007: The Physical Science Basis. Contribution of Working Group I to the Fourth Assessment Report of the IPCC*, Cambridge University Press, 2007.
- Stommel, H. (1961) Thermohaline convection with two stable regimes of flow, *Tellus*, **13**, 224–230.

Keywords

Attractor

- Random
- Strange

Bifurcation(s)

- Diagram
- Hopf
- Pitchfork
- Saddle-node
- Successive

Dynamical systems

- Autonomous
- Deterministic
- Ergodic theory of dynamical systems
- Geometric theory of dynamical systems
- Nonautonomous
- Random

Energy balance models (EBMs)

Equilibria

- Multiple
- Stable
- Unstable

General circulation models (GCMs)

- Atmospheric
- Oceanic
- Coupled

Lorenz model

Measure

- Invariant
- Sample

Modeling hierarchy

- Zero-dimensional (0-D) models
- One-dimensional (1-D) models
- Two-dimensional (2-D) models
- Three-dimensional (3-D) models

Noise

- additive
- multiplicative

Oscillations

- Intraseasonal
- Interannual
- Interdecadal
- Self-sustained

Radiation

- Incoming, shortwave, solar
- Outgoing, long-wave, terrestrial

Radiative-convective models

Stochastic process

Thermohaline circulation
Global overturning
Local convection

Symbols and units

b – normalized wavenumber [nondimensional]
 c – heat capacity
 d – thermal diffusion coefficient [nondimensional]
 D – horizontal heat flux
 m – grayness factor [nondimensional]
 Q_0 – solar radiation at the top of the atmosphere
 r – normalized Rayleigh number
 P_r – Prandtl number
 R_i – incoming radiation
 R_o – outgoing radiation
 s, t, τ – time [depends on time scale of interest: s, day or years]
 S – salinity [‰]
 T – temperature [deg K]
 x, y, z – spatial coordinates
 X, Y, Z – generic dependent variables [nondimensional]
 α – (planetary) albedo [nondimensional]
 β, γ – constant coefficients in Eq. [10] [nondimensional]
 $\delta t, \Delta t$ – time step and time interval, respectively [nondimensional]
 λ_{ao} – atmosphere–ocean coupling coefficient [nondimensional]
 μ – control parameter [nondimensional]
 ν – invariant measure
 ρ – density
 σ – Stefan–Boltzmann constant
 σ_0 – noise intensity = standard deviation [nondimensional]
 τ_1, τ_2 – pullback times [nondimensional]; see Fig. 4

N.B. All variables are in SI units, except where otherwise indicated.

Suggested cross-references

All other articles under the general rubric of **Climate Variability**.
El Niño–Southern Oscillation (ENSO)
Global Change
Ocean Circulation
Paleoclimatology
Weather Regimes and Multiple Equilibria

Figure Captions

Figure 1. Bifurcation diagram for the solutions of an energy-balance model (EBM), showing the annual-mean temperature \bar{T} vs. fractional change of insolation at the top of the atmosphere μ . The arrows pointing up and down at about $\mu = 1.4$ indicate the stability of the branches: towards a given branch if it is stable and away if it is unstable. The other arrows show the hysteresis cycle that global temperatures would have to undergo for transition from the upper stable branch to the lower one and back. The angle γ gives the measure of the present climate's sensitivity to changes in insolation. [After Ghil and Childress (1987) with permission from Springer-Verlag.]

Figure 2. Diagram of an Atlantic meridional cross section from North Pole (NP) to South Pole (SP), showing mechanisms likely to affect the thermohaline circulation (THC) on various time-scales. Changes in the radiation balance $R_{in} - R_{out}$ are due, at least in part, to changes in extent of Northern Hemisphere (NH) snow and ice cover, V , and how they affect the global temperature, T ; the extent of Southern Hemisphere ice is assumed constant, to a first approximation. The change in hydrologic cycle expressed in the terms $P_{rain} - P_{evap}$ for the ocean and $P_{snow} - P_{abl}$ for the snow and ice is due to changes in ocean temperature. Deep-water formation in the North Atlantic Subpolar Sea (North Atlantic Deep Water: NADW) is affected by changes in ice volume and extent, and regulates the intensity C of the THC; changes in Antarctic Bottom Water (AABW) formation are neglected in this approximation. This in turn affects the system's temperature, and is also affected by it. [After Ghil *et al.* (1987) with permission from Springer-Verlag.]

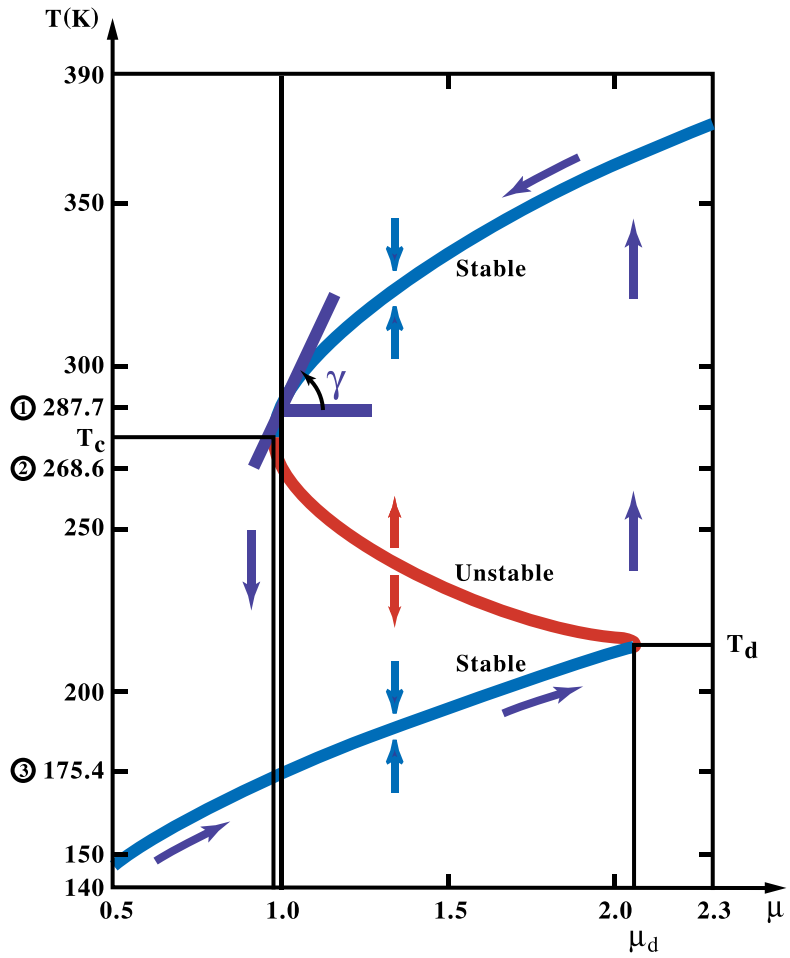
Figure 3. Dependence of THC solutions on two parameters in a hybrid coupled model; the two parameters are the atmosphere–ocean coupling coefficient λ_{ao} and the atmospheric thermal diffusion coefficient d . (a) Schematic regime diagram. The full circles stand for the model's stable steady states, the open circles for stable limit cycles, and the solid curve is the estimated neutral stability curve between the former and the latter. (b) Hopf bifurcation curve at fixed $d = 1.0$ and varying λ_{ao} ; this curve was obtained by fitting a parabola to the model's numerical-simulation results, shown as full and open circles. [From Chen and Ghil (1996) with permission from the American Meteorological Society.]

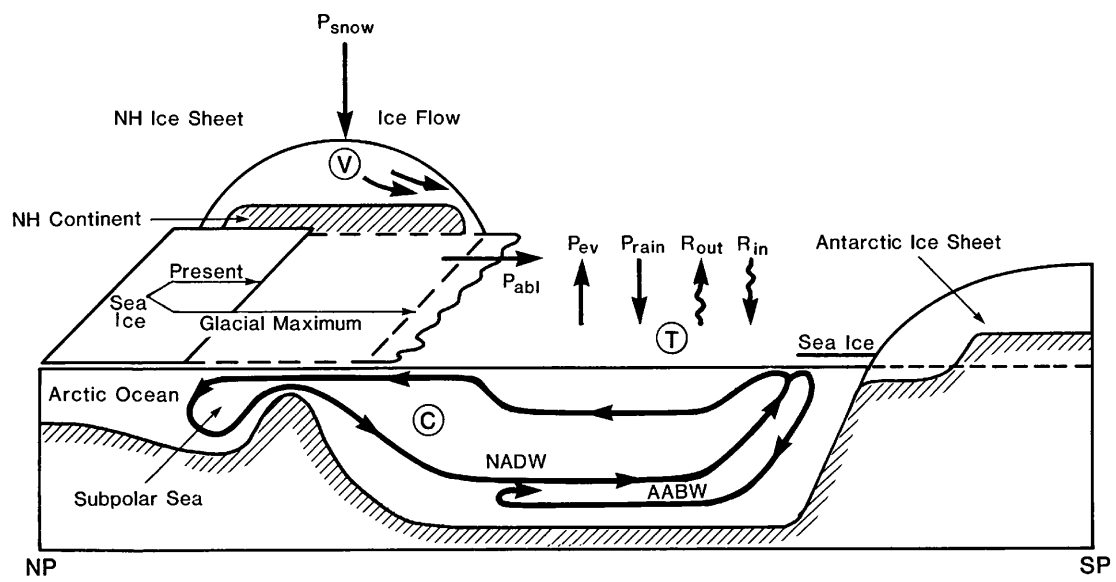
Figure 4. Schematic diagram of a random attractor $A(\omega)$ and of the pullback attraction to it; here ω labels the particular realization of the random process $\theta(t)\omega$ that drives the system. We illustrate the evolution in time t of the random process $\theta(t)\omega$ (solid black line at the bottom); the random attractor $A(\omega)$ itself (yellow band in the middle) with the “snapshots” $A(\omega) = A(\omega; t = 0)$ and $A(\omega; t)$ (the two vertical sections, heavy solid); and the flow of an arbitrary set B from “pullback times” $t = -\tau_2$ and $t = -\tau_1$ onto the attractor (heavy blue arrows). [After Ghil *et al.* (2008) with permission from Elsevier.]

Figure 5. Four snapshots of the stochastically perturbed Lorenz (1963) model's random attractor $A(\omega)$ and the invariant measure $\nu(\omega)$ supported on it. The parameter values are the classical ones — normalized Rayleigh number $r = 28$, Prandtl number $P_r = 10$, and normalized wavenumber $b = 8/3$ — while the noise intensity is $\sigma_0 = 0.5$ and the time step is $\delta t = 5 \times 10^{-3}$. The color bar used is on a log-scale and quantifies the probability to end up in a particular region of phase space; shown is a projection of the three-dimensional phase space (X, Y, Z) onto the (X, Z) plane. Notice the complex, interlaced filament structures between highly (yellow) and moderately (red) populated regions. The time interval Δt between two successive snapshots — moving from left to right and top to bottom — is $\Delta t = 0.0875$. Note that the support of the invariant measure $\nu(\omega; t)$ may change quite abruptly, from time t to time $t + \Delta t$; see the related short video. Weakly populated regions cover an important part of the random attractor and are, in turn, entangled with regions that have near-zero probability (black). [After Chekroun *et al.* (2011) with permission from Elsevier.]

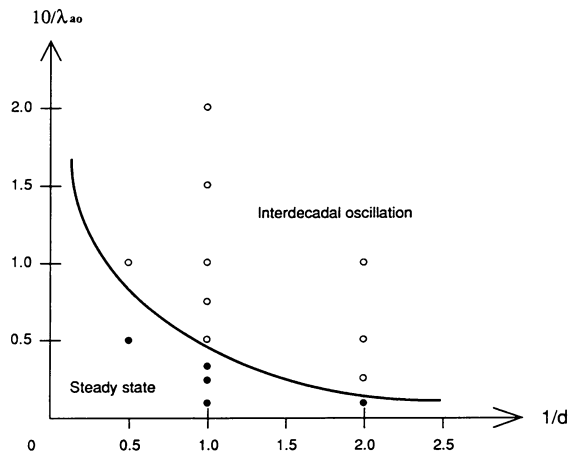
Video 1. Short segment from the evolution in time of the Lorenz model's random attractor $A(\omega)$ and of the invariant measure $\nu(\omega)$ supported on it; same parameter values as in Fig. 5. Each frame is generated like the four snapshots in Fig. 5, i.e. it shows the probability density of the points that land in a particular domain of the phase space, when launched from a homogeneous distribution of points in a ball that contains the strange attractor of the classical, deterministic Lorenz (1963) model. There are two types of motion present in the video: First, a pervasive “jiggling” of the overall structure that can be traced back to the roughness of the driving noise process and to the multiplicative way it enters into the stochastically perturbed version of the Lorenz model. Second, there is a smooth and

quite regular low-frequency motion present in the evolution of the sample measures, which is driven by the deterministic system's flow on the two lobes of the deterministic system's strange attractor.

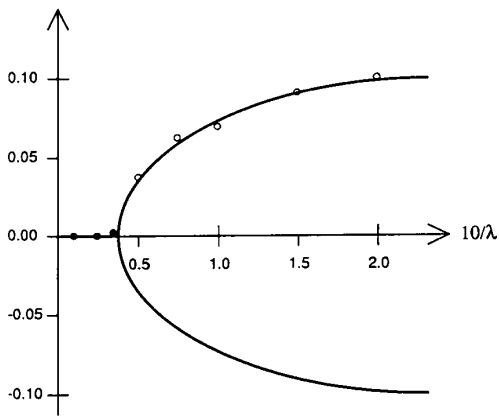




a) Regime diagram



b) Bifurcation diagram



Pullback attraction to $A(\omega)$

